Lappeenranta University of Technology
School of Engineering Science
Computational Engineering and Technical Physics

**Timo Paappanen**

# EFFECT OF HUMIDITY ON ELECTRIC POTENTIAL OF $SNO_2$ FILM INVESTIGATED BY KELVIN PROBE FORCE MICROSCOPY

Master's Thesis

Examiners: Professor Erkki Lähderanta, M.Sc Ekaterina Soboleva

# ABSTRACT

Lappeenranta University of Technology
School of Engineering Science
Computational Engineering and Technical Physics

Timo Paappanen

**Effect of humidity on electric potential of $SnO_2$ film investigated by Kelvin probe force microscopy**

Master's Thesis

2020

31 pages, 15 figures, 1 table.

Examiners: Professor Erkki Lähderanta, M.Sc Ekaterina Soboleva

Keywords: Material physics, Kelvin probe force microscopy, $SnO_2$, Hygroelectricity

In this study hygroelectric behaviour of an $SnO_2$ sample was studied using Kelvin probe force microscopy (KPFM) and humidity controlling equipment. The objective was to detect any possible surface potential changes within scans, and furthermore any possible patterns to the potential changes by analysing data from multiple different sets of scans. Due to time limitations only one sample could be scanned and it could not be ensured that the scans could be taken from the same area. Analysis of the results revealed potential changes individually within each scan set. However no common pattern to the variation were found.

# PREFACE

Firstly I would like to thank professor Erkki Lähderanta for giving me the opportunity for being a part of this study and supporting me throughout my studies in LUT. I also want to thank Ekaterina Soboleva for helping me with getting familiar with the equipment and answering my questions. I also would like to express my gratitude to my friends and family for encouraging me throughout my studies.

Lappeenranta, June 16, 2020

*Timo Paappanen*

# CONTENTS

# LIST OF ABBREVIATIONS

| | |
|---|---|
| AFM | Atomic force microscopy |
| AC | Alternating current |
| AM-KPFM | Amplitude modulation - kelvin probe microscopy |
| CPD | Contact potential difference |
| EDS | Energy dispersive spectroscopy |
| FM-AFM | Frequency modulated atomic force microscopy |
| FM-KPFM | Frequency modulation - kelvin probe microscopy |
| KPFM | Kelvin probe force microscopy |
| PF KPFM | Peak force Kelvin probe force microscopy |
| PC | Personal computer |
| RH | Relative humidity |
| SEM | Scanning electron microscopy |
| SPM | Scanning probe microscopy |
| USB | Universal serial bus |

# 1 Introduction

## 1.1 Background

In the usual sense, one can get the impression that in high humidity environments charge would dissipate. However, in a study committed in 2008 it was observed that under controlled relative humidity negative ions can accumulate on cellulose film from positive potential of an acrylic sheet [1]. Ever since, hygroelectricity, the phenomenon where electric potential in a material changes based on the exposed humidity, has been in a growing interest in the scientific community.

In two previous works, done by Rasheed Anum [2] and Nafiseh Mohammadi [3], zirconium oxide crystals were studied using Kelvin probe force microscopy (KPFM) and scanning electron microscopy (SEM) to study their hygroelectric behaviour. The present work seeks to expand the previous studies by measuring a sample using KPFM and analysing the results.

## 1.2 Structure of the thesis

This thesis starts with an introductory part. In section three the research equipment and software are described as an overview, including atomic force microscopy (AFM), KPFM and the humidity controlling system used alongside. In section three the samples and their general physical properties are introduced. In the fifth section the measurement procedure and details are presented including any special notices. In the sixth section the results of the scans are analysed and interpreted, and the analysing procedure is described. In the final section conclusion over the analysed results are discussed, along with possible further studies. In addition, all references are listed after the main text for reviewing.

## 1.3 Objectives and delimitations

In the present thesis the main objective is to detect and measure potential changes in a $SnO_2$ sample using KPFM, and to find any possible relations between different factors such as mean surface potential and humidity. Humidity is measured by the same system that was used in Rasheed's thesis [2]. Due to constraints, calibration process is mostly left out and relative humidity values are used instead. In addition due to time constraints only one sample could be measured and it could not be ensured that the same area was scanned in each set of scans.

# 2 Related work

This thesis mainly seeks to expand the work based on two other studies done on the same topic. First one is master's thesis done by Rasheed Anum [2], in which $ZrO_2$ nanocomposite was studied using the same KPFM scanning system used in this work. The second one is master's thesis made by Nafiseh Mohammadi [3], which also carried out a similar study of voltage behaviour of $ZrO_2$ nanoparticles in different humidities and temperatures using SEM imaging and energy dispersive spectroscopy (EDS).

# 3 Methodology

## 3.1 Atomic Force Microscopy

AFM is a form of scanning probe microscopy (SPM) that utilizes interaction between a scanned material and a scanning probe to form an image of the surface. AFM systems generally consist of three basic parts: a cantilever with a tip (probe), a laser and a piezoelectric scanner. During operation, sample is moved underneath the scanning probe, which depending on the topology of sample surface, bends from the short range forces, which causes changes in the deflection of the laser that hits the probe. This is registered by a photodetector,

and can be used to construct an image of the scanned surface. A simplified diagram of this system is depicted in figure 1.

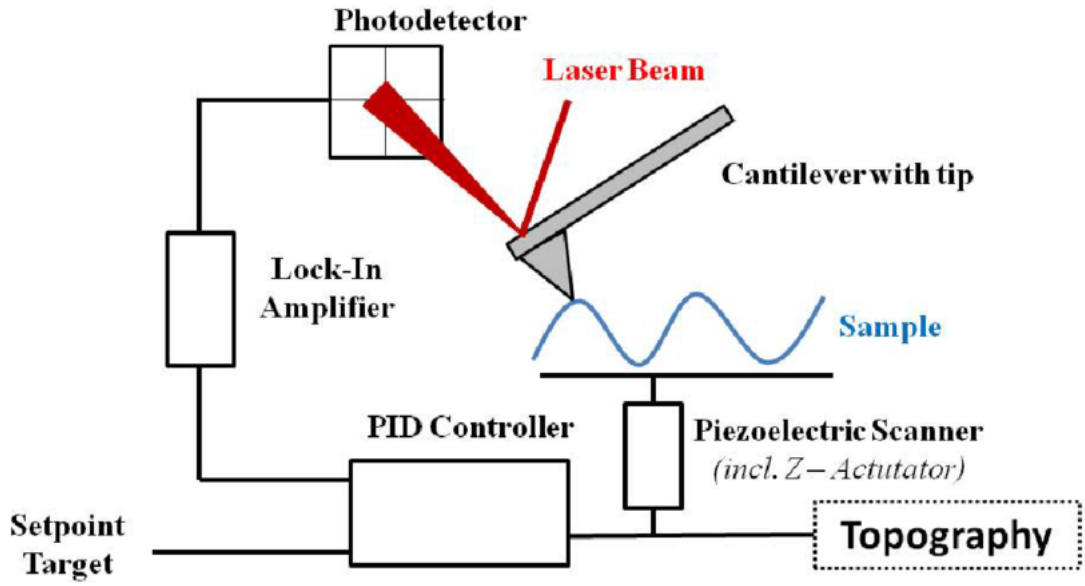


**Figure 1.** A simplified diagrammic representation of an AFM setup [4]

The resolution of AFM devices depends on multiple factors, with the most important including tip diameter and external noise such as vibrations. In the right conditions the resolving power can be in the order of nanometers, compared to hundreds of nanometers of optical microscopes that are limited by the diffraction limit. This along with techniques such as frequency modulated atomic force microscopy (FM-AFM) allows materials to be scanned on atomic scale resolutions [5].

Second factor that affects the resolution of AFM is presence of artefacts. The image is formed by the surface-cantilever interaction forces instead of light. Therefore, AFM is subject to its own type of artefacts caused by various factors. Firstly, as the tip diameter has a finite size instead of being point like, features in the scanned images can appear larger than they are in reality. The finite tip diameter also affects AFM scans due to topological effects [6]. As this factor is dependent on the probe itself, it can be minimized by improving the quality of the probe. Secondly, external vibrations may affect the quality of scans. The smaller the scan size is and the higher the resolution, the more prevalent artefacts caused by external vibrations are. Minimizing these are done by using a specialized anti-vibrational table to hold the AFM system in place. In addition, the scans can be done in a time and place where the amount of external vibrations are as low as possible.

In addition, thermal drift is another possible source of artefacts where changes of external temperature cause changes in the mechanical properties of the imaging system [7]. These can be minimized by stabilizing the temperature in the scanning environment to the best possible extent. By understanding these artefacts and their origin, it is possible to improve understanding of AFM data and even potentially remove them without affecting real data.

Data collected by AFM is divided into multiple individual channels, each representing their own type of data. The most important of these is surface height, which represents the topology of the scanned area. KPFM also allows surface potential to be recorded from its corresponding channel. Additional channels usually used for checking the integrity of the data such as deformation, phase and amplitude can also be recorded.

There are multiple modes of SPM. The one used in this thesis is KPFM. Figure 2 shows the AFM setup Multi Mode 8 provided by Bruker Corporation that was used in this work, including the scanner (1), optical microscope (2) and personal computer (PC) used for operating the system.

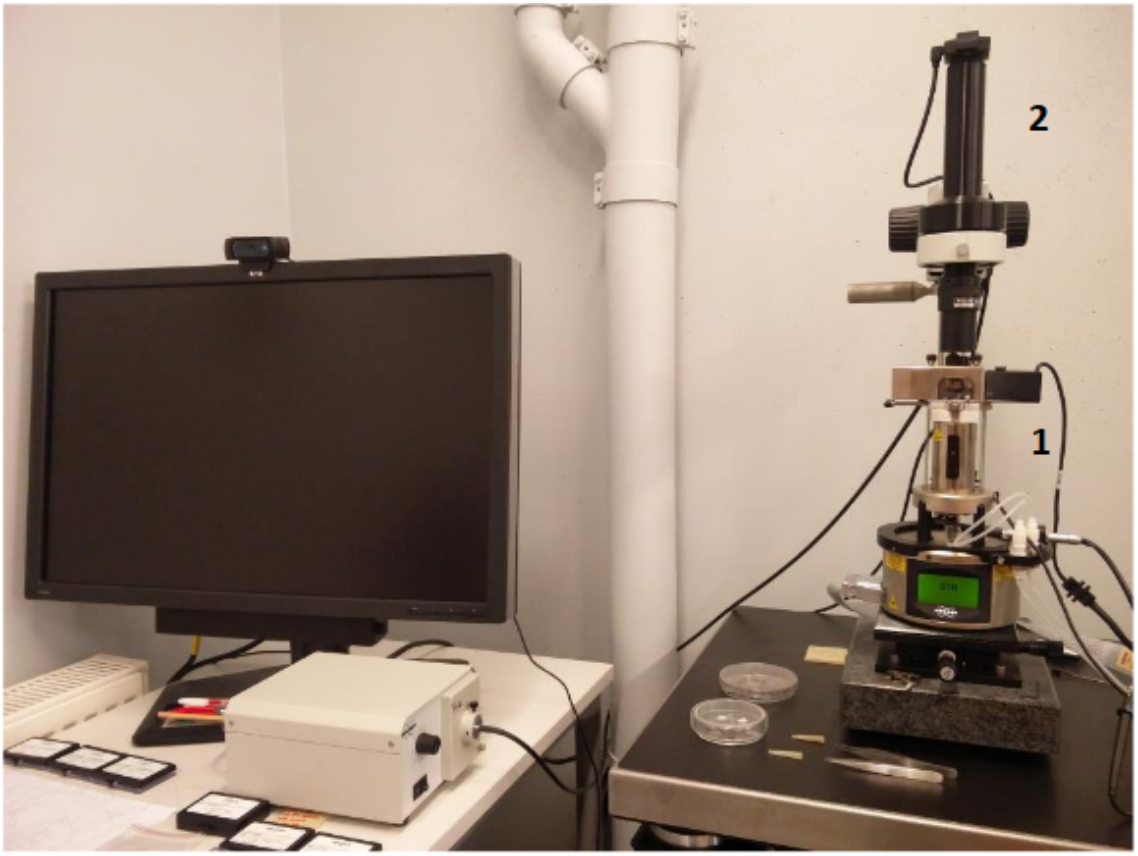


**Figure 2.** The AFM Multi Mode 8 (Bruker Co.): scanner (1) and optical microscope (2)

As the probe is relatively fragile in terms of macro-scale interactions, the quality of the probes might degrade over time during their lifetime. The quality of a probe can be checked by calculating parameters, such as quality factor $Q$, which can be expressed in the form of equation 1.

$$Q = \frac{f_0}{\Delta f}. \tag{1}$$

Here $f_0$ is the resonant frequency of the probe and $\Delta f$ is the resonance width, or full width at half maximum. This number represents the energy losses within the probe can vary in the range of around 0 to 1000, with higher numbers representing better quality. With the KPFM probes used in this work, the scale of this factor ranges usually in the scale of 0 to 500.

### 3.1.1 Piezoelectric scanner

The scanner of the AFM consists of a controllable piezoelectric ceramic tube. By controlling the voltage of the connected electrodes (see fig. 3), the tube can be either bent in a plane or retracted/extended in the z direction perpendicular to the movement plane. Using this movement, a sample can be scanned by first extending the tube in such a way that the sample touches the probe, and then moving the sample under the probe by controlling the voltage of the electrodes on the sides.

The controlling software is carefully calibrated in such a way that the correct movement of the sample is ensured, because the extension and contraction of the tube is not completely linear in terms of voltage.

The equation of the piezoelectric effect can be expressed in the format of equation 2.

$$u_{ij} = d_{ijk} \cdot E_k. \tag{2}$$

where $u_{ij}$ is strain tensor, $E_k$ is electric field component, and $d_{ijk}$ are components of the piezoelectric coefficient tensor that depend on the ceramic material used. There are in total 18 components on the 3x6 piezoelectric matrix, of which $i$, $j$ and $k$ denote. On the strain tensor $i$ and $j$ denote the axial components of the strain.

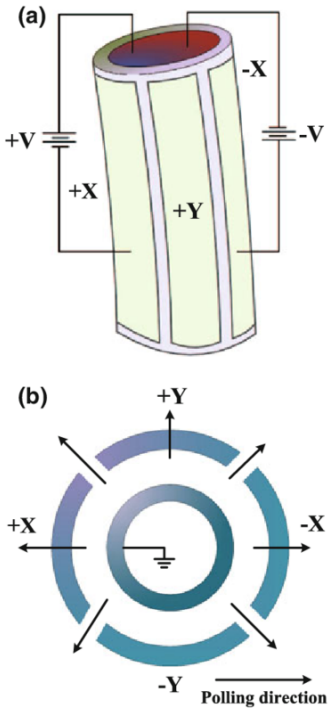


**Figure 3.** Illustrative diagram of the piezoelectric scanner tube. (a) side view and (b) top view [8].

### 3.1.2 Kelvin Probe Force Microscopy

KPFM is a more specialized mode of AFM. This mode of SPM is able to map surface potential of the scanned sample. Compared to standard AFM, a KPFM probe is conductive, which reveals a potential difference on the sample. This allows the measurement of surface potential. This ability to measure small scale potential differences over a surface makes it useful for the context of the present work, where the fine behaviour of potential is important.

The working principle of KPFM is based on the work function of moving an electron out of a surface, e.g. over a vacuum from a metal tip to sample surface. In case of KPFM, measuring the potential becomes a task of measuring contact potential difference (CPD), which can be considered as the work function. Figure 4 illustrates three different cases: separated sample and tip (a), contact between sample and tip (b) and external bias between sample and tip (c).

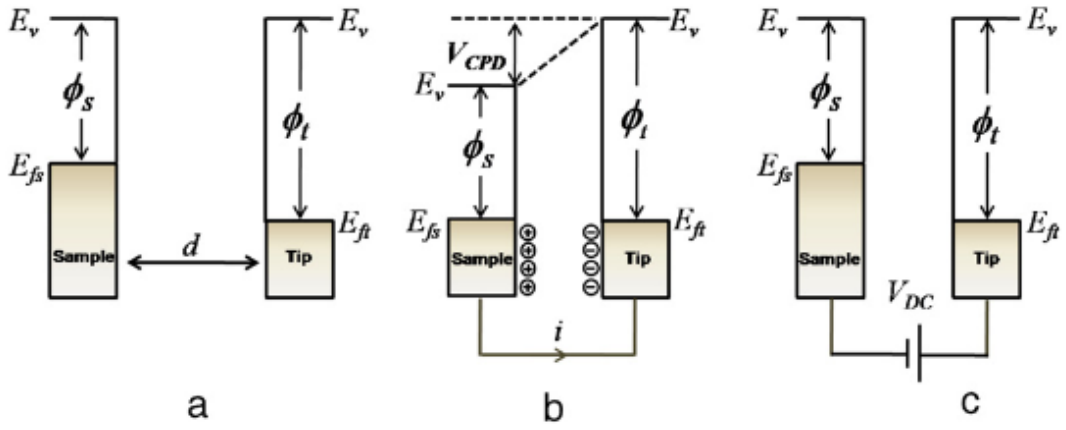


**Figure 4.** A diagram of the working principle of KPFM [9]. Three different cases are presented: (a) Separated sample and tip, (b) contact between sample and tip, (c) external bias ($V_{DC}$) is applied between sample and tip.

The CPD between the tip and the sample can be described by equation.

$$V_{CPD} = \frac{\phi_{tip} - \phi_{sample}}{-e}. \tag{3}$$

Here $\theta_{tip}$ and $\theta_{sample}$ are the work functions for the tip and the surface of the sample respectively, and *e* represents the charge of an electron.

This difference is strongly affected by the distance between the sample and the tip. As the tip is brought closer to the sample, electric force appears due to Fermi energy level differences between the sample and the tip.

As dictated by the Lennard-Jones potential (fig. 5), when the tip approaches a surface, the first force is attractive. After a certain point this force changes to a repulsive interaction until the tip touches the sample surface. The same happens in reverse when moving the tip away from the surface.

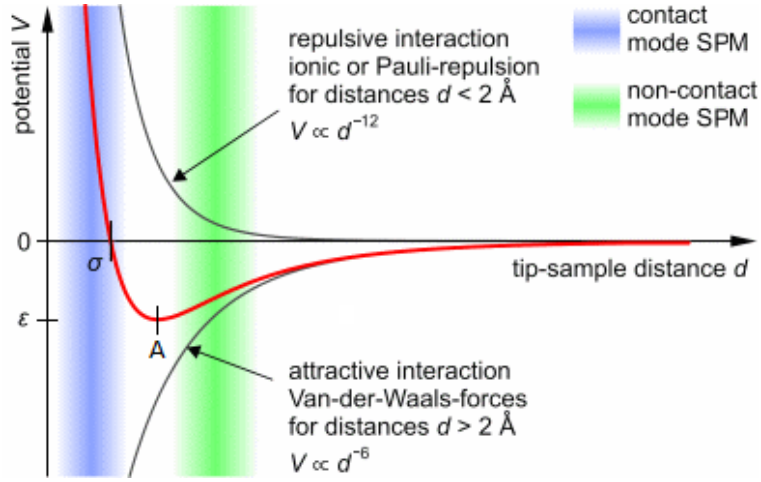


**Figure 5.** V(d) graph that describes Lennard-Jones potential between a scanning probe microscope (SPM) tip and a sample [10].

Generally, the resolution of KPFM compared to standard AFM is lower due to the increased tip radius caused by the conductive metal coating of the probe.

The cantilever oscillation is induced by an AC bias between the sample and the probe. This frequency is usually the cantilevers resonant frequency, which also is usually listed in probe specifications. This frequency is obtained during the calibration process that is done before the beginning of measurements to take into account miniature case-by-case differences caused by differences in the installation process of the cantilever.

The scales of a typical KPFM probe are very small: dimensions of the cantilevers are usually within micrometers and mass within the scale of $10^{-10}$ kg. Due to normal operational forces also being very small (in the order of $10^{-7}$ - $10^{-12}$ N), care should be taken when handling KPFM probes. More specifically, any interference with the scanning equipment during any ongoing scan should be avoided to prevent noise in the scan results, or in the worse case damage of the probe itself due to contact with the surface that is scanned.

**PeakForce KPFM** is a special form of KPFM microscopy developed by Bruker. It is a combination of frequency modulated KPFM (FM-KPFM) and PeakForce tapping mode AFM, in which tapping is done below the resonant frequency of the cantilever to avoid filtering effect and dynamics of a resonating system [11]. This provides advantages over FM-KPFM such as ability to identify possible artefacts caused by tip-sample contact by observing changes in scans when changing lift height. In this work, the usual advantages of FM-KPFM for imaging at small scales are largely not used due to the relatively large

size of the scans (1.5 μm at smallest), PeakForce KPFM (PF-KPFM) is opted to be used in this work.

## 3.2 Humidity controller and sensor

In order to control the humidity during the experiments, a dedicated system consisting of pressure valves to control dry air flow, a bubbler and a measuring circuit was used (fig. 6).

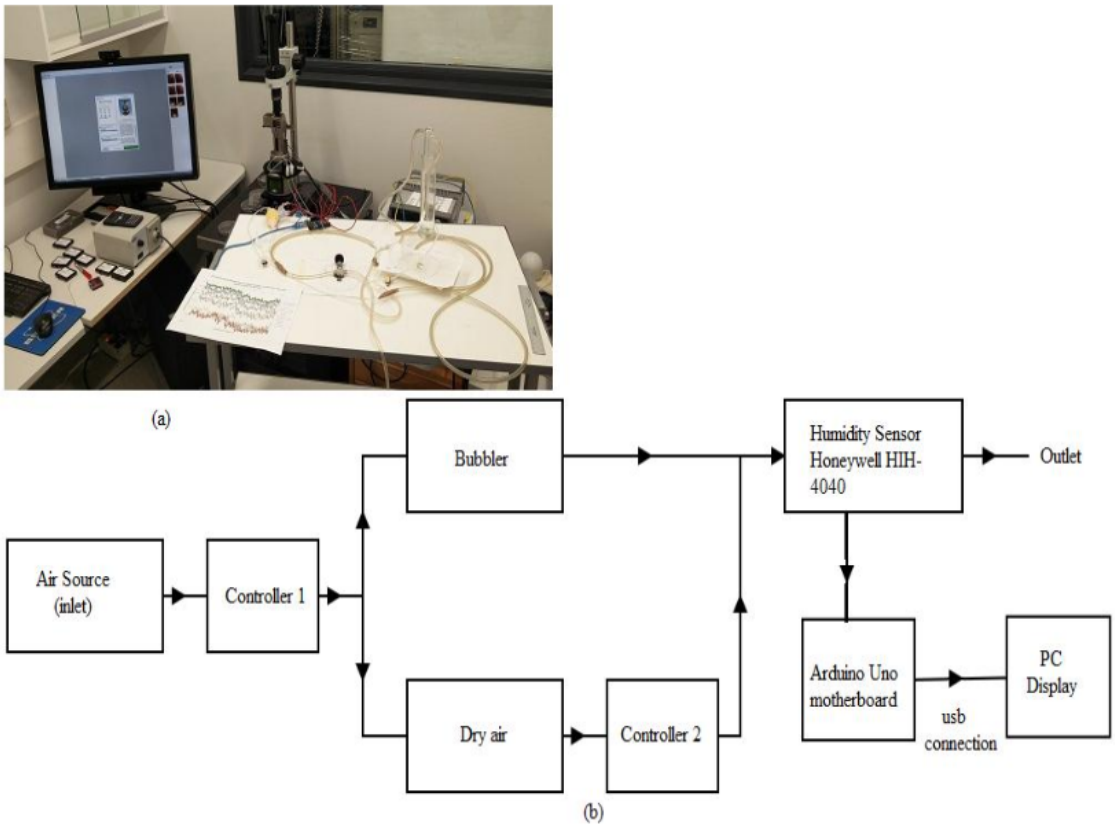


**Figure 6.** The experimental set-up and b) Schematic diagram of the humidity controlling system that was used [2].

The circuit board is an Arduino Uno board by Arduino, an open source electronics platform [12]. The board includes a script running in order to measure the humidity within the sealed sensor section (a Honeywell HIH-4040 sensor was used). The PC connected to the board by universal serial bus (USB), a humidity reading is periodically displayed using the following .ino script that was uploaded on the circuit board. According to the datasheet of

a related Honeywell sensor (HIH-4000), an accuracy of $\pm 3.5\%$ RH is expected at room temperature (25 °C) [13].

The probe holder for the measurements was a special sealed system that had a humidity controlling device attached. This controller system consisted of a water containing flask, a pressure releasing valve, pressurized air source and a humidity sensor.

The system has 2 main ways of controlling the humidity in the AFM gas cell (fig. 7): adjusting the air flow controlling valve, and opening/closing the secondary valve. Using these two valves, the humidity in the gas cell was adjusted in the range of 0-70%.

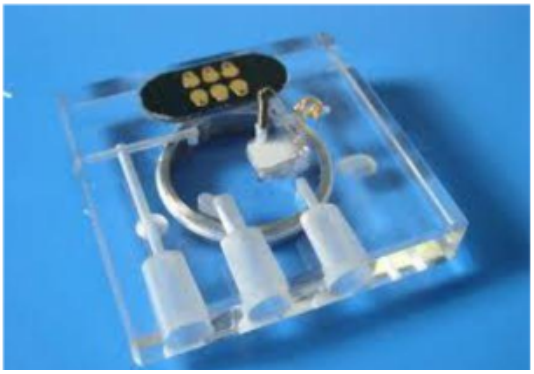

**Figure 7.** Image of the special gas cell probe holder that was used [2].

The humidity sensor was not perfect, as it had leaks along with the gas cell. These are not taken quantitatively into account within the calculations presented here, but are kept in mind when analysing and interpreting the results.

As the sample is expected to have microscopic change of dimensions with humidity changes, the probe was withdrawn from the sample while any major changes in humidity were done in order to prevent damage to the probe due to probable stresses from pressing the sample.

## 3.3 Software

The software used in this thesis consists of three main parts: AFM controlling software, humidity sensor software and image analysis software. The Nanoscope software used for controlling the AFM device and Nanoscope Analysis image processing software are

provided by Bruker. This controller software includes methods and an automated control for calibrating AFM probes, scanning and saving data using the AFM hardware. The analysis software includes functions used for analysing and processing data taken using the AFM system, such as removing/minimizing artifacts, and overviewing data from different channels. In this work the most relevant image processing tools were flattening, plane fit and line removal.

The humidity sensor software is a script ran using Arduino, an open source single-board hardware and software platform. The following code was uploaded and ran on the Arduino Uno board to print a humidity reading on a console for reviewing during and after scans.

In addition, GNU octave, an open source mathematical programming language [14] was used for plotting and analysing the data points exported from Nanoscope analysis.

```
#include <dht.h>

dht DHT1;
dht DHT2;

#define ANALOG_PIN A0
#define DHT1_PIN 6
#define DHT2_PIN 7

//float ANALOGSTEP = 3. / 1024; // MAXOUTPUT VOLTAGE = 5V *
   0.7952 = 3.976V

int chk1 = 0;
int chk2 = 0;
int analogSens = 0;

void setup(){
  Serial.begin(9600);
}

void loop()
{
// chk1 = DHT1.read11(DHT1_PIN);
// Serial.print("T1 = ");
// Serial.print(DHT1.temperature); //was Serial.println
// Serial.print("; H1 = "); // 145 at 100%, ~110% for 90%
   because of nonlinear absorption
```

```
// Serial.print((DHT1.humidity)*10/6 - 13); // 0.6339 -
   8.2953/0.6339

// chk2 = DHT2.read11(DHT2_PIN);
// Serial.print(" | T2 = ");
// Serial.print(DHT2.temperature - 3); // dumb calibration of
   temperature by just minus 2 deg
// Serial.print("; H2 = "); // 137 at 100%, ~100% for 90%
   because of nonlinear absorption
// Serial.print((DHT2.humidity)*19/10 - 39); // 0.5248 -
   19.4060/0.5248

  analogSens = (analogRead(ANALOG_PIN)/1024.0) * 5 * 30.28073 -
     32.5705;
  // Old line was "analogSens = (analogRead(ANALOG_PIN)/1024.0 -
     0.16)/0.0062;"
  // On Nov2 we changed it into "analogSens =
     (analogRead(ANALOG_PIN)/1024.0) * 5 * 30.28073 - 32.5705;"
  Serial.print(" | AH = ");
  Serial.println(analogSens);

  delay(3000);
}
```

# 4 Samples

Before measuring the real sample, a test sample provided by Bruker (fig 8) was used to calibrate the probe to check the quality and efficiency of the probe. This sample is patterned with Au, Si and Al strips.

**Figure 8.** Image of a test Al-Si-Au sample that is used for calibrating a KPFM probe similar to the one used in this work [15].

After a probe of desired quality was found, the real sample was installed for measurement. The sample is composed of thin $SnO_2$ film obtained by magnetron sputtering in argon plasma on direct current, with a tin metal plate of diameter 42 mm and purity of 99.99% as a sputtering target. A diagram of a sputtering deposition system is displayed in figure 9.

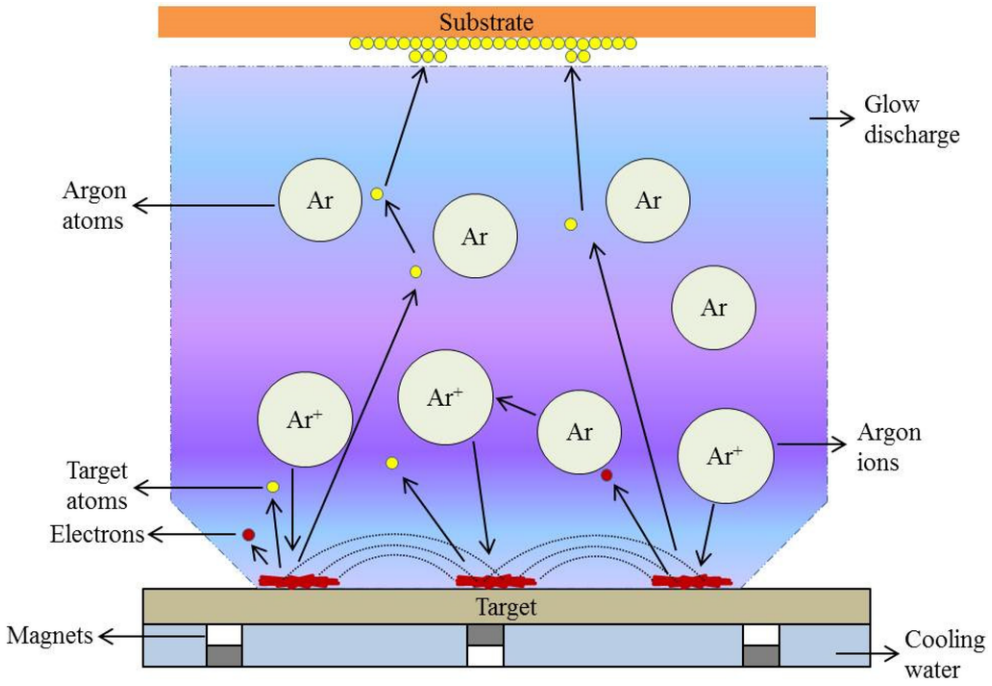


**Figure 9.** A diagram that represents a sputtering deposition system. The sputtering target is bombarded with sputtering Ar gas, which causes microscopic Sn particles to escape, after which they attach on the substrate [16].

For the sputtering process, a metal nickel strip of (diameter 3 mm) was mounted on the Sn targets surface, and the distance between the substrate and target was set to 2 cm. After sputtering the obtained tin films were subjected to two-stage oxidative annealing in air. In the first stage the film was heated up to 200 C and had isothermal annealing for 2 hours. In the second stage the sample was heated up to 400 C and had isothermal annealing for 1 hour.

# 5 Experiments

For each of the independent set of scans, the KPFM system was calibrated using the built-in functions and meters of the hardware and software. The setup procedure included the following steps:

- Set up silicon tube for humidity sealing
- Install sample
- Install the probe holder with a probe
- Bring down the probe
- Align laser onto cantilever and photodetector
- Use the tuning options in software to find the resonant frequency of the cantilever

Additionally in order to increase the strength of the signal on the potential channel, the scanning distance was decreased from the default setting to 40 nm.

After setting up the sample in the gas cell and after calibrating the laser, the samples were first scanned in a 10x10 micrometer area in room humidity (19% according to the humidity sensor) with a resolution of 40 nanometers. After this, a smaller area of 1.5x1.5 micrometers was selected and scanned with the same probe in room humidity (17-21%), at 40% and 80% (max). In addition, scans at 40% and room humidity were repeated after the maximum humidity scan to investigate any potential changes from reducing humidity. An optical image of the area scanned in the first set of measurements is shown in fig. 10.

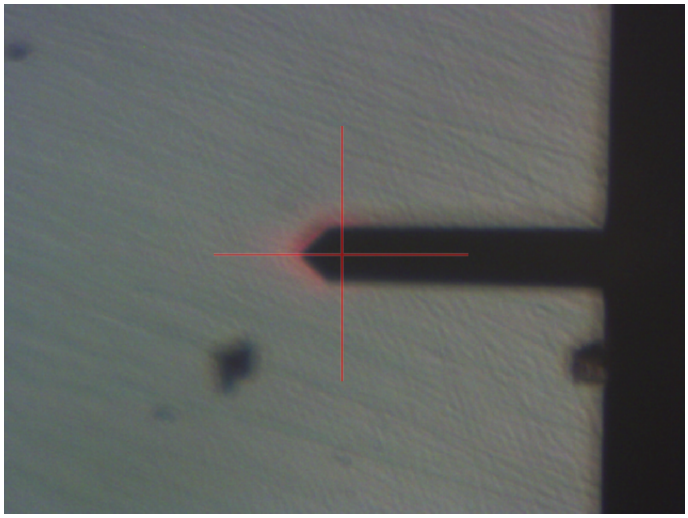

**Figure 10.** Optical microscope image of the area measured in the first set of scans. Also the cantilever can be seen as a black silhouette.

For analysis, the relative humidity values were scaled so that maximum humidity equals 100%. As the maximum absolute humidity was 80%, all humidity values were multiplied by a factor of 1.25.

Setting the humidity to a certain value was done by turning the pressure valve to a more opened or closed position until the desired value was reached. After 2 minutes of humidity stabilization, the valve was closed and the air seal on the gas seal was closed as quickly as possible to prevent humidity from leaking out, while taking care not to disrupt the AFM set-up. As the cell was not perfectly airtight, a decrease in humidity was observed and recorded in each of the measurements that were done. In total the sample was scanned 3 times.

Due to limiting factors such as lack of procedure to align the probe to the same area between measurements, it could not be ensured that the scans were done from the same spot of the sample. Instead this was taken into account in analysis.

# 6 Analysis of the data

Data from the sample were sorted in tables for basic overview and comparison. The data scales of height channel images were also adjusted to match each in order to directly compare topology of scans so that height changes can be seen. In addition, the scans were also aligned by topographical features for easier comparison of potential differences between scans.

Due to the sensitivity and noisiness of the potential channel data, image processing was applied only to height channel data. The height channel processing was done using the procedure described below:

Firstly, using the NanoScope analysis software, a plane fit of 1st order was applied separately on X and Y axes, which removes tilt by fitting the data on applied axis to linear equations $z = a + bx$ and $z = a + by$ respectively. After this, the "flatten" algorithm was run at 0th order, which removes scan line misalignment by centring data on each line using polynomial $z = a$. In cases where there were still line artifacts left, the "erase line" -algorithm was executed for each of the artifact lines until the image was cleared.

After processing each of the images, direct comparisons could be executed between the obtained images and data. First observation was that the range of potential changes between the cases, with some measurements having overall higher potential values than others. Usual range was from around 100 mV to 400 mV, when in some cases the minimum ranged under -100 mV.

Using this methodology, the potential range of the scans were generally within the range of about 110 - 400 mV. However, there were also some scans with the lower range of potential reaching as low as -250 mV.

A common area of the sample was selected for further analysis after the image processing was ready. Potential was analysed using the "rotating box" -tool in Nanoscope Analysis, which selects an area of interest from a scan and prints a graph based on average of points along horizontal axis. This provided a common reference area for each of the scan sets where the same corresponding area was scanned. A 1500 nm x 200 nm area shown in figure 11 was chosen for the first scan.

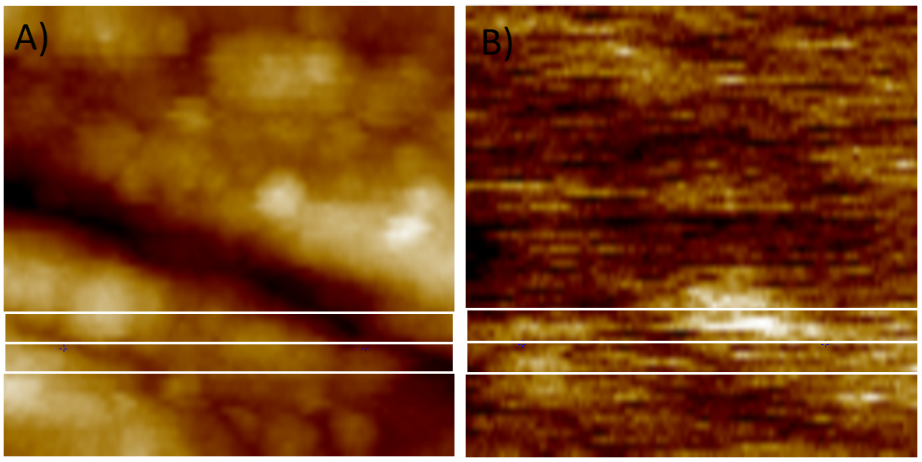


**Figure 11.** The area that was chosen for data points to be exported in the first scan set viewed from height channel (A) and the same area viewed from potential channel (B). The box outlined by white lines mark the 1500x200 nm area selected for obtaining potential data. The total area of the whole images are 1500 nm x 1500 nm.

Because the first 1.5 µm room humidity scan in the first set of scans was located in different area than the other 1.5 µm scans in the same set, a separate area for this scan was selected to compare potential changes.

After selecting a common area from each of the scans, raw data was printed out from each scan using data export function and was plotted on a graph using GNU octave for direct comparison. Firstly the exported data was plotted with potential as a function of distance as seen in figure 12.

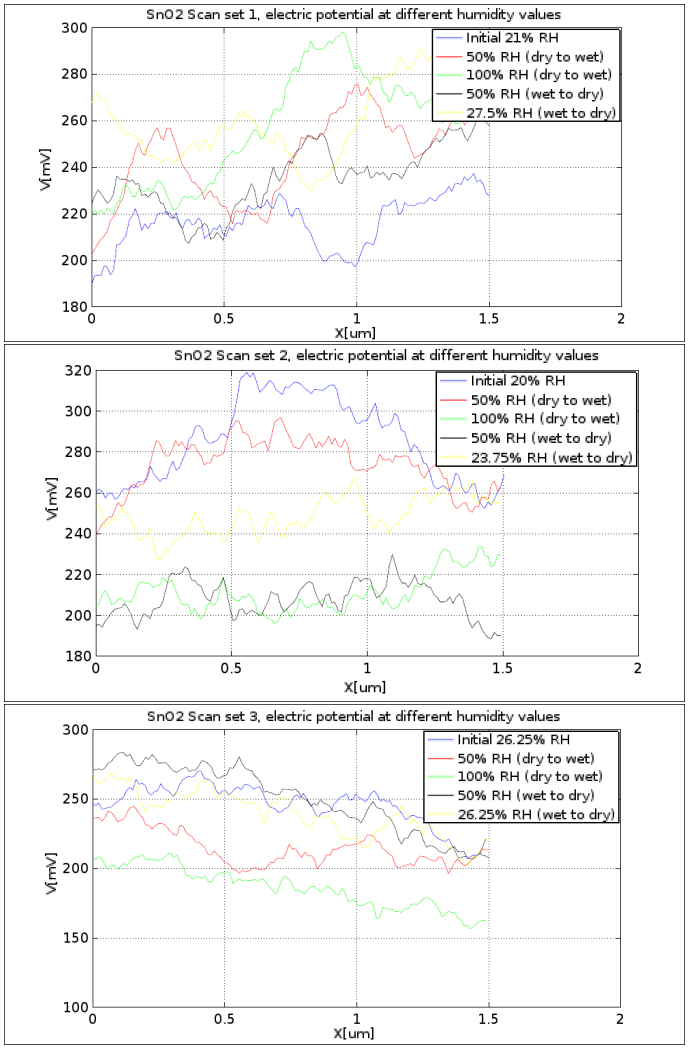


**Figure 12.** V(x) plots of data exported from all three sets of scans.

These plots show variation within the overall results. Firstly, the overall range of potential can be seen to vary within a range of 150 mV to 320 mV. The results in the second and first set have mostly higher potential than the third set.

In addition, overall potential changes vary greatly between the three sets; in the first set 100% RH (green line) shows overall higher potential values compared to other RH values, while in the second and third sets 100% RH has overall the lowest potential values. Similar difference can be seen also with 50% RH wet-to-dry (black line) and initial room humidity scans (blue line). These major differences can be seen also in figure 13 where all scans with initial room humidity (A), 100% RH (B) and 50% RH (wet to dry) are plotted in the same graphs.

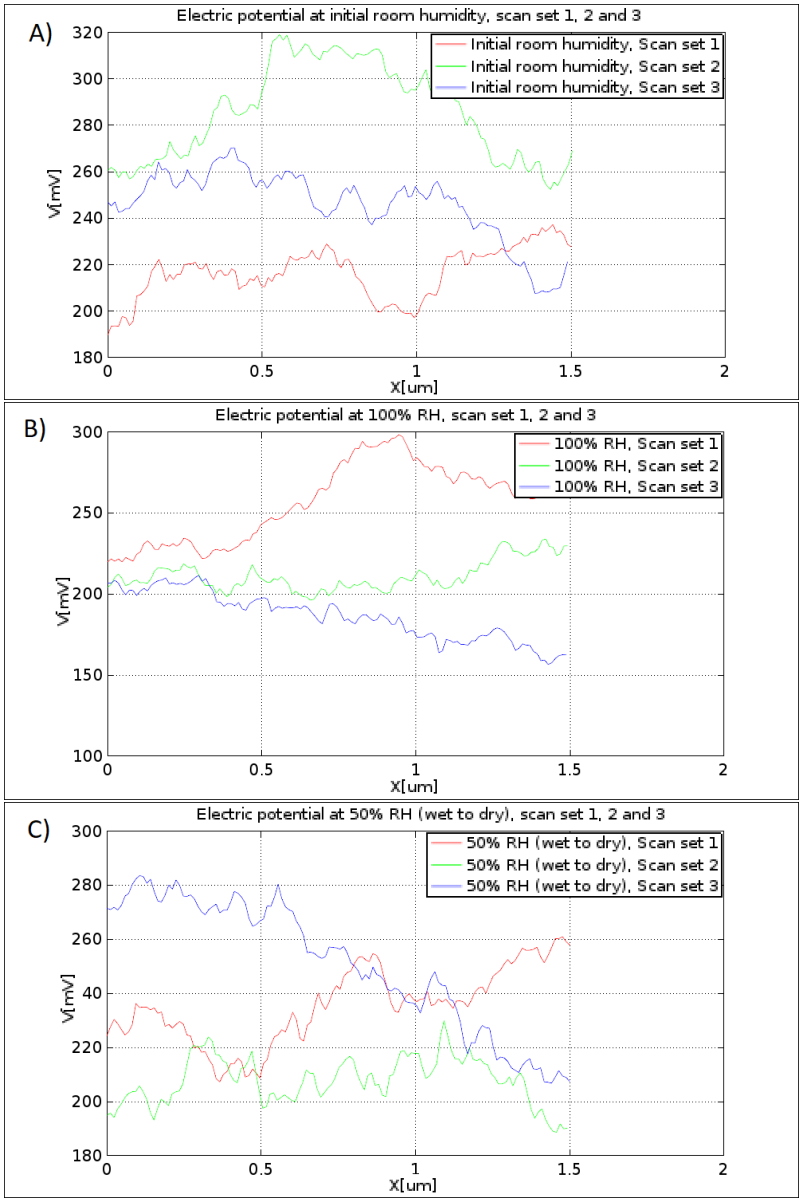


**Figure 13.** Plots of exported data with scans taken in same humidity state in same graphs. Initial room humidity state (A), 100% RH (B) and 50% RH wet-to-dry (C).

In order to compare average and most common surface potential levels, the potential data was plotted into histograms for each set of scans. In figure 14 in each plot the potential values are divided into 30 equally sized bins and displayed on the same graph for easier visual comparison.

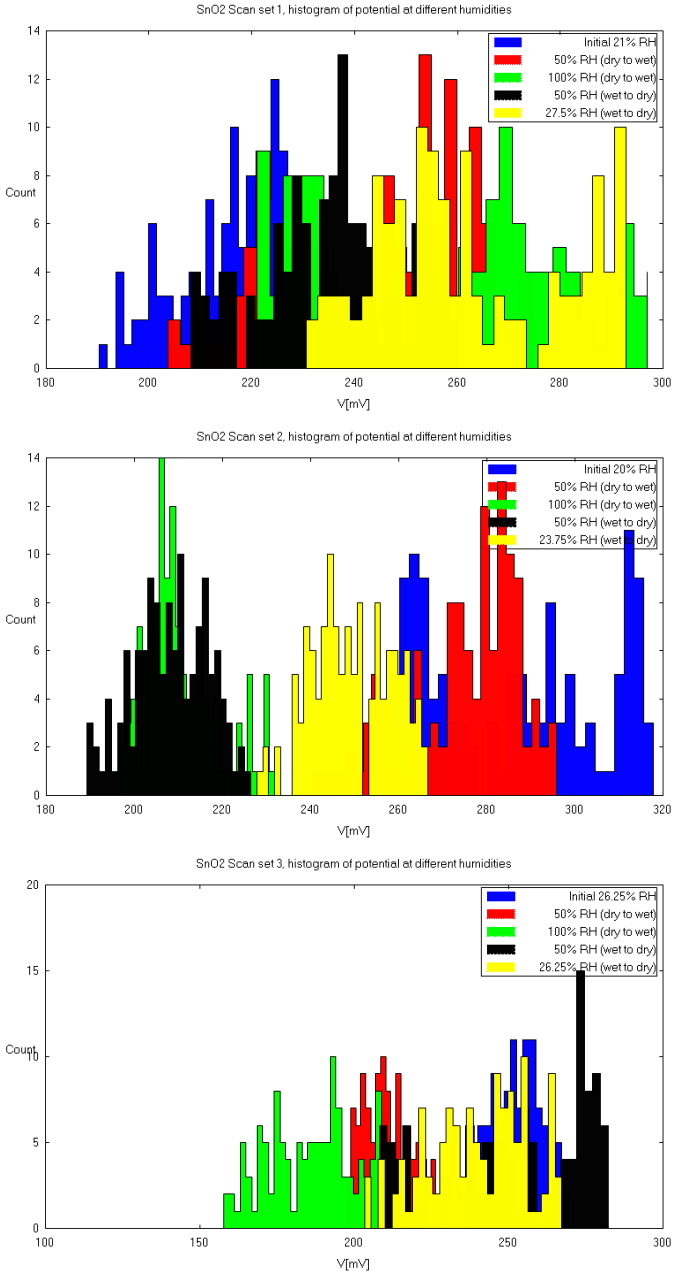


**Figure 14.** Histograms of potential values of each set of scans, with values divided into 30 bins.

The same phenomenon of varying measurements between sets of scans observed in the V(x) plots can also be observed within these histograms, with RH values representing overall lowest and highest potential values varying between scans.

Finally for a direct numeric comparison, average and median potential values from the exported data were also calculated for each individual scan. It was found that the averages were very similar to median values (maximum difference being 4 mV). The average

values were plotted to 2 dimensional plots in figure 15. The average values for scans are marked as individual points, with the horizontal axis representing scan number; initial room humidity, 50% RH, 100% RH, 50% RH wet to dry and room humidity wet to dry are represented as points of x = [1, 2, 3, 4, 5] respectively. As with previous plots, variations within average potential levels can be observed, but no clear common trend between the changes were observed other than the average potentials varying within a range of around $240 \pm 40$ mV.

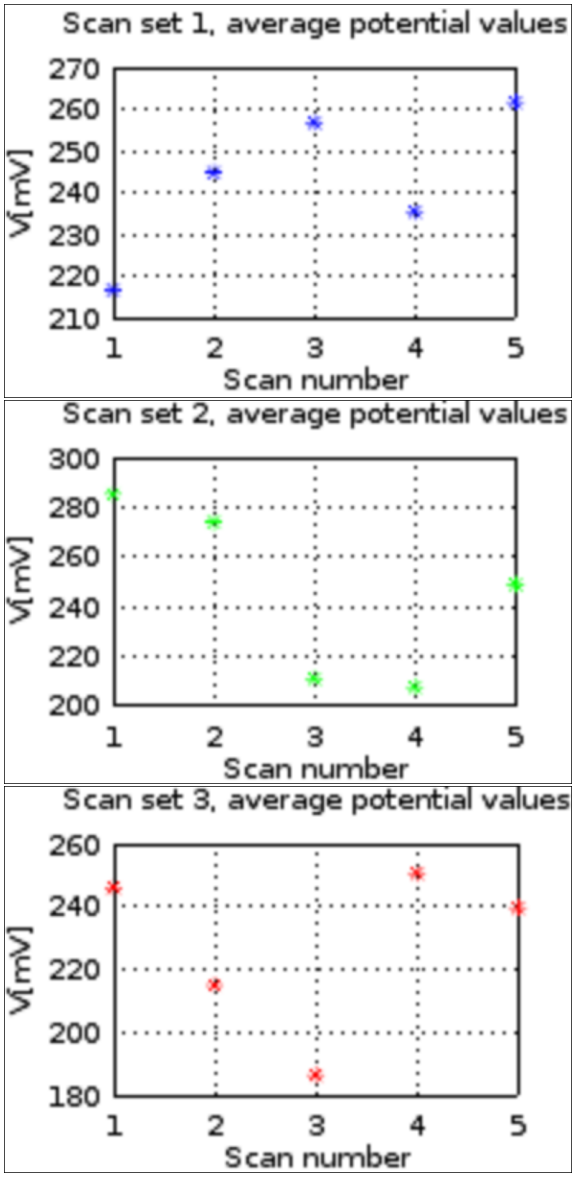


**Figure 15.** Average potential plotted as function of scan sets where the horizontal axis represents the scan order number. Respective humidity values for scan numbers are [room humidity, 50%, 100%, 50%, room humidity] respectively, with 4 and 5 being wet to dry scans.

## 6.1 Current study

The hypothesis was that the potential of the sample changes with humidity changes. Considering the histograms in figure 14, there seems to be varying potential values between each scan within a set. However, when looking at multiple sets of scans (fig. 14), do not reveal a definitive pattern for these variances, with no RH value representing the highest or lowest observed potential values overall.

This discrepancy can be due to multiple possible factors. Firstly, it could not be ensured that the scans were taken from the same area, even within a single set of scans as was the case within the first set. Therefore it is possible that the non-correlating potential changes might be caused by different behaviour between each area scanned. In addition, as the scans were taken apart multiple days between each other, it is possible that external factors can have affected the sample, such as storage space humidity changes.

Additional possible explanation for this behaviour is that the observed not correlating changes in potential value is an intrinsic property of the measured $SnO_2$ sample. This could be verified or discarded by taking additional measurements from the same area of the sample and comparing the results obtained in this study.

## 6.2 Future work

As in terms of statistical terms the number of test replications was small, one scanned sample with 3 sets of 5 scans. The results of this study could be expanded by increasing the sample size to reduce the effects of error. In addition taking care of scanning the same area between multiple scans could also decrease the effect of error for more conclusive results as discussed in the previous section.

Further reduction of error could be possible by using better sealing for the gas cell to ensure humidity stays constant during scanning process.

# 7 Conclusion

The supplied $SnO_2$ sample was systematically measured using KPFM in this thesis after learning how to operate the provided hardware and software including the AFM scanning system, KPFM, humidity controller and sensor, and the analysis software. The surface potential values of the provided $SnO_2$ sample were observed to vary in a range of around [150 mV, 320 mV]. Due to multiple possible factors, such as not being able to ensure the scanning the same area, no definitive pattern for these changes could be found.

# REFERENCES

[1] Soares, and Bertazzo, Sergio and Burgo, Thiago and Baldim. A new mechanism for the electrostatic charge build-up and dissipation in dielectrics. *Journal of the Brazilian Chemical Society*, 19, 2008.

[2] Anum Rasheed. Effect of humidity on electric potential of $ZrO_2$ nanocomposite investigated by AFM/KPFM. Master's thesis, Lappeenranta University of Technology, Finland, 2017.

[3] Nafiseh Mohammadi. Humidity to electricity converter based on zirconia nano particles. Master's thesis, Lappeenranta University of Technology, Finland, 2017.

[4] Paul Narchi. *Investigation of crystalline silicon solar cells at the nano-scale using scanning probe microscopy techniques*. PhD thesis, 12 2016.

[5] Takeshi Fukuma, Kei Kobayashi, Kazumi Matsushige, and Hirofumi Yamada. True atomic resolution in liquid by frequency-modulation atomic force microscopy. *Applied Physics Letters*, 87(3), 2005.

[6] Minhwan Lee, Wonyoung Lee, and Fritz B Prinz. Geometric artefact suppressed surface potential measurements. *Nanotechnology*, jun 2006.

[7] Davide Ricci and Pier Carlo Braga. *Recognizing and Avoiding Artifacts in AFM Imaging*. 2004.

[8] Sajal Das, Hemanshu Pota, and Ian Petersen. *Intelligent Tracking Control System for Fast Image Scanning of Atomic Force Microscopes*, volume 581, pages 351–391. 12 2014.

[9] Wilhelm Melitz, Jian Shen, Andrew C. Kummel, and Sangyeob Lee. Kelvin probe force microscopy and its application. *Surface Science Reports*, 66(1):1 – 27, 2011.

[10] Holger Schönherr and Gyula Vancso. *Atomic Force Microscopy in Practice, Scanning Force Microscopy of Polymers*. 01 2010.

[11] Stefan B. Kaemmer. Application note 133 introduction to bruker's scanasyst and peakforce tapping afm technology. `https://www.bruker.com/fileadmin/user_upload/8-PDF-Docs/SurfaceAnalysis/AFM/ApplicationNotes/Introduction_to_Brukers_ScanAsyst_and_PeakForce_Tapping_Atomic_Force_Microscopy_Technology_AFM_AN133.pdf`, 2011. Accessed: 2020-06-15.

[12] Arduino introduction page. https://www.arduino.cc/en/Guide/Introduction. Accessed: 2020-04-25.

[13] Honeywell hih-4000 datasheet. https://sensing.honeywell.com/honeywell-sensing-hih4000-series-product-sheet-009017-5-en.pdf. Accessed: 2020-04-25.

[14] Gnu octave. https://www.gnu.org/software/octave/about.html. Accessed: 2020-05-19.

[15] Bruker AFM probes, PF-KPFM test sample. https://www.brukerafmprobes.com/a-3822-pfkpfm-smpl.aspx. Accessed: 2020-06-15.

[16] Devendra Maurya, A. Sardarinejad, and Kamal Alameh. Recent developments in r.f. magnetron sputtered thin films for ph sensing applications—an overview. *Coatings*, 4:756–771, 12 2014.